Applied Microbiology and Biotechnology (2022) 106:2729–2738
https://doi.org/10.1007/s00253-022-11855-9

METHODS AND PROTOCOLS

New dynamic microreactor system to mimic biofilm formation and test anti-biofilm activity of nanoparticles

Natalia Bourguignon[1,2] · Vivek Kamat[1] · Maximiliano Perez[1,2] · Kalai Mathee[3,4] · Betiana Lerner[1,2] · Shekhar Bhansali[1]

Received: 15 November 2021 / Revised: 21 February 2022 / Accepted: 26 February 2022 / Published online: 24 March 2022

Abstract

Microbial biofilms are composed of surface-adhered microorganisms enclosed in extracellular polymeric substances. The biofilm lifestyle is the intrinsic drug resistance imparted to bacterial cells protected by the matrix. So far, conventional drug susceptibility tests for biofilm are reagent and time-consuming, and most of them are in static conditions. Rapid and easy-to-use methods for biofilm formation and antibiotic activity testing need to be developed to accelerate the discovery of new antibiofilm strategies. Herein, a Lab-On-Chip (LOC) device is presented that provides optimal microenvironmental conditions closely mimicking real-life clinical biofilm status. This new device allows homogeneous attachment and immobilization of *Pseudomonas aeruginosa* PA01-EGFP cells, and the biofilms grown can be monitored by fluorescence microscopy. *P. aeruginosa* is an opportunistic pathogen known as a model for drug screening biofilm studies. The influence of flow rates on biofilms growth was analyzed by flow simulations using COMSOL® 5.2. Significant cell adhesion to the substrate and biofilm formation inside the microchannels were observed at higher flow rates > 100 µL/h. After biofilm formation, the effectiveness of silver nanoparticles (SNP), chitosan nanoparticles (CNP), and a complex of chitosan-coated silver nanoparticles (CSNP) to eradicate the biofilm under a continuous flow was explored. The most significant loss of biofilm was seen with CSNP with a 65.5% decrease in average live/dead cell signal in biofilm compared to the negative controls. Our results demonstrate that this system is a user-friendly tool for antibiofilm drug screening that could be simply applied in clinical laboratories.

Key Points

- *A continuous-flow microreactor that mimics real-life clinical biofilm infections was developed.*
- *The antibiofilm activity of three nano drugs was evaluated in dynamic conditions.*
- *The highest biofilm reduction was observed with chitosan-silver nanoparticles.*

Keywords Microreactor · Nanoparticles · Continuous flow · Biofilm · Microfluidics

Introduction

Biofilms are composed by microorganisms' communities enclosed in a self-synthesized extracellular polymeric matrix or substances (EPS), composed of proteins, lipids, polysaccharide nucleic acids, which attach to abiotic or abiotic surface in the solid–liquid interface. This EPS also impedes antimicrobial's access to the bottom layer cells, resulting in increased multidrug resistance. Apart from EPS components, cell-to-cell communication, i.e., quorum sensing, performs an important role in the faster progression and pathogenesis of the biofilm community (Singh et al. 2019). *Pseudomonas aeruginosa* is a Gram-negative opportunistic pathogen recognized for its proclivity to form biofilms (Mulcahy et al. 2014). It is a notoriously

Natalia Bourguignon and Vivek Kamat contributed equally to this work.

✉ Kalai Mathee
matheek@fiu.edu

✉ Betiana Lerner
belerner@fiu.edu

[1] Department of Electrical and Computer Engineering, Florida International University, Miami, FL 33174, USA

[2] IREN Center, National Technological University, Haedo, 1706 Buenos Aires, Argentina

[3] Department of Human and Molecular Genetics, Herbert Wertheim College of Medicine, Florida International University, Miami, FL 33199, USA

[4] Biomolecular Sciences Institute, Florida International University, Miami, FL, USA

resistant bacterium that is much feared in clinical settings (Andersson 2003; Thi et al. 2020). Infections with *P. aeruginosa* can be fatal in immune-compromised and cystic fibrosis patients (Maurice et al. 2018). It is one of the most common biofilm generators in "chronic wounds" that are wounds without healing in 3 months (Drago et al. 2019; Sutlief et al. 2019). The National Institutes of Health, USA, reported that biofilm formation causes more than 80% of wound complications and infections (Qayyum and Khan 2016). As well, biofilm formation plays a significant risk role during the osseointegration process, as well as tissue regeneration (Souza et al. 2021). Many research efforts are dedicated to the eradication of biofilm in healthcare (Bowler et al. 2020). Some approaches employed so far to control biofilm formation in healthcare settings are the development of biofilm inhibitors based on the understanding of the molecular mechanism of biofilm formation and to modify the biomaterials in medical devices to prevent biofilm formation (Subhadra et al. 2018). Numerous modification techniques of biomaterials, introducing chemical functional groups to surface, have been adopted to produce functionalized biomaterial surface with biological properties and for clinical applications (Kyzioł et al. 2017).

A vital attribute of the biofilm lifestyle is the intrinsic drug resistance imparted to bacterial cells protected by the matrix. Bacterial cells encapsulated within the biofilm require nearly 1000 times the antimicrobial concentration necessary to kill their living unicellular planktonic counterparts (Brandenburg et al. 2018). Inconsistencies between several in vitro studies (Coenye et al. 2007; Spittaels and Coenye 2018) argue the need for experimental setups that approach in vivo conditions. An actual wound site has numerous dynamic events such as flowing wound exudates, increased blood flow at the wound site, increased temperature, etc. A continuous culture in the microfluidic devices that we propose can close approximation to in vivo conditions.

Since biofilm is difficult to eradicate, alternate treatment strategies, including the use of different antibacterial nanomaterials, have been explored (Qayyum and Khan 2016; Benoit et al. 2019). These nanomaterials, specifically metallic silver nanoparticles (SNPs) (Ganem-Rondero et al. 2018), have been effectively used in wound dressings (Negut et al. 2018; Choudhury et al. 2020). SNPs, chitosan nanoparticles (CNP), and chitosan-coated SNPs (CSNP) (Soledad et al. 2019) were selected for the present study. These SNPs possess a broad spectrum of antibacterial properties and have been previously investigated (Vu et al. 2018; Singh et al. 2019; Affes et al. 2020; Choudhury et al. 2020), but their interaction in a fluid flow condition (akin to a pus environment) remains unclear. The application of SNPs against biofilms will deliver understandings into the mechanism of biofilm response and regulation, help to fight biofilm resistant infections, and contribute to improving human health.

Microfluidics devices are identified as Lab On a Chip (LOC), and they consist of a network of microchannels that incorporate different sections, chambers, columns, and reservoirs (Whitesides 2006). The LOC application for the study of microorganisms and their microenvironment is an emerging field that has not been widely explored until now (Illath et al. 2021). The benefits of the miniaturization of the system offer new opportunities. In particular, accurate spatiotemporal control across the microenvironments of organisms in combination with high-resolution images monitoring provide a unique view of biological events. These innovative techniques open new ways to study the environment and organisms, allowing an excellent approximation to the environmental conditions. It is possible to study at the level of a single cell or biofilm (micron level) (Stanley et al. 2016; Burmeister et al. 2019).

This article proposes a microfluidic device as a tool that mimics the real-life clinical environment to study biofilm formation and antibiofilm activity using nanoparticles (NPs) in continuous-flow conditions. In this work, we have developed and explored a microfluidic platform to study *P. aeruginosa* biofilm formation and evaluate nanoparticle-based treatments. This study's long-term goal is to assess nanoparticle efficacy as an anti-biofouling agent and its use in wound healing via smart wound bandages.

Materials and methods

Bacterial strain

Green fluorescent–labeled *Pseudomonas aeruginosa* PA01-EGFP (Wu et al. 2000) was used in all the experiments. EGFP strain allows in situ biofilm analysis using fluorescence microscopy because it is a mutant form of GFP with high fluorescence properties (Sutlief et al. 2019). The strain was kept at – 20 °C in LB broth (% m/v: tryptone 1.0; yeast extract 0.5; NaCl 1.0; pH 7.0) added with 20% (v/v) glycerol. Before experiments, the microorganism was propagated in LB broth at 37 °C in an orbital shaker at 200 rpm for 24 h, and it was used as inoculum in all experiments.

Synthesis of silver, chitosan, and silver-chitosan nanoparticles

The silver nanoparticles (SNPs) were synthesized using silver nitrate (99.99% pure, Sigma) with sodium borohydride ($NaBH_4$ 99% pure) and tri-sodium citrate (99.99% pure) as reducing and capping agent, respectively. For all the experiments, solutions were prepared in Milli-Q grade deionized water (Millipore). A 100-mL 3 M solution of silver nitrate

was prepared and mixed with 10-mL 1 M sodium citrate solution (capping agent). A 5-mL 2×10^{-3} M sodium borohydrides solution was added progressively to the solution. The color of the solution turns golden yellow which visually confirms reduction reaction and synthesis of SNP (Vu et al. 2018).

The chitosan nanoparticles (CNPs) were synthesized using the ionic gelation method (Kamat et al. 2016). Briefly, chitosan 0.5 mg/mL (Sigma, Cat no: 448877) (deacetylation degree < 75%) was prepared in 1% glacial acetic acid (Sigma, Cat no: 695092) and sodium tripolyphosphate 0.2 mg/mL (TPP, Sigma Cat no:238503) in deionized water. The TPP (1.25 mL) was added dropwise with a micropipette to 5 mL of 0.5 mg/mL chitosan solution, under magnetic stirring (1000 rpm) at room temperature, keeping the ratio of chitosan to TPP 2.5:1(Kamat et al. 2016).

The synthesis of silver-chitosan nanoparticles (CSNP) was carried out using 0.5 mg/mL pre-synthesized SNPs prepared using the above method and mixed with chitosan solution of the same concentration. The solution was allowed to mix at 500 RPM for 30 min, and 0.2 mg/mL TPP solution was added in a dropwise manner to get the final concentration of 0.5 mg/mL CSNP. The crosslinking between TPP and chitosan polymer encapsulated silver nanoparticles. After adding the TPP solution, the mixture was stirred for another 30 min. Synthesized NPs were characterized for particle size, zeta potential, and UV Vis-absorbance using Malvern Dynamic Light Scattering (DLS) and Thermo fisher UV-V spectrometer (Thermo Fishers, USA).

Chips for biofilm studies: design and manufacture

Layout Editor software was used for the architecture microchannels design (KLayout 2018). The microchip design involves four channels (496 µm width) with four cisterns each (1690 µm width), one inlet and one outlet (Fig. 1). The microchannel design has 28 µL as a total internal volume. The channel height is 150 µm, and curved wave channels were designed to avoid cells' accumulations in square corners and the formation of bubbles (Peñaherrera et al. 2016). The high relief design mold was manufactured using a 150-µm-thick SU-8 photolithographic pattern (Peñaherrera et al. 2016). A silicon wafer (Virginia Semiconductor, Inc.), used as the substrate, was cleaned by sonication in acetone and isopropyl alcohol and dehydrated for 10 min at 200 °C on a hotplate. Then, SU-8 negative photoresist (Microchem) was dispensed on the silicon wafer and spin in two identical cycles. The spinner was ramped at 100 rpm/s from zero to 500 rpm to spread the resin; this speed was held for 5 s. In the spin cycle, the spinner was ramped at 300 rpm/s from zero to 3000 rpm, and this speed was held for 30 s. The resin was soft baked at 65 and 95 °C for 3 and 6 min, respectively. The substrate was aligned, and the resin was exposed to UV

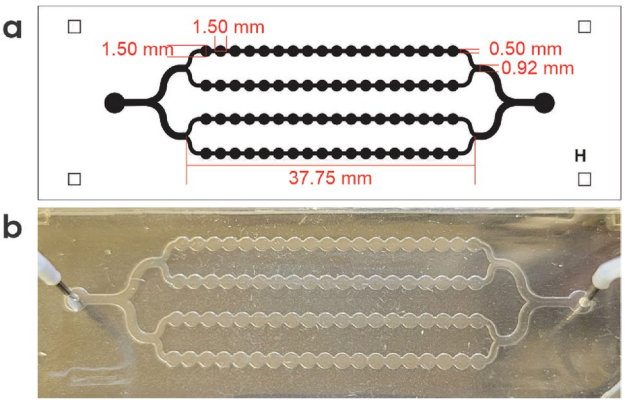

Fig. 1 Microfluidic device for antibiofilm susceptibility testing. **a** Microchannels design and dimensions and **b** PDMS device with tubing connections

at 250 mJ/cm^2. The resin was post-exposure baked at 65 and 95 °C for 1 and 6 min, respectively. Finally, the SU-8 resin was developed for 10 min under agitation.

The microdevices were built using polydimethylsiloxane (PDMS; Sylgard 184, Dow; Corning) on the top and glass on the base. The PDMS microfluidic device manufacturing technique was previously described (Peñaherrera et al. 2016; Bourguignon et al. 2018). The PDMS replica was cut and unmolded, and 1-mm-diameter fluidic connection ports were punched. By exposure to oxygen plasma for 3 min (BD 10AS, Chicago, USA), the PDMS replica was irreversibly attached to a glass substrate. Finally, the setup was completed by assembling with the tubing and connected to a peristaltic pump.

Computational fluid dynamics characterization

To investigate the effects of the dynamic flow on bacterial growth and biofilm formation in the microchip, we developed a model using COMSOL 5.2 to study the flow field at the experimentally relevant flow rate of 50, 75, 100, and 150 µL/ min. We selected these flow rates as they coincide with a blood flow rate in wound sites ranging from 50 to 110 µL/ min for 1 g tissue. The resting capillary blood flow velocity is reported to be ~ 0.65 mm^3/s at skin temperature of 30.4 °C, corresponding to 0.04 mL/min (Stücker et al. 1996). The computational calculation was based on the Navier–Stokes equations, and due to the very low Reynolds number in microfluidic devices, the inertial component was neglected, allowing a higher mesh density for computation. Boundary conditions for the 3D model included water properties for flowable materials, zero pressure at the outlet, progressive laminar flow, and no-slip. From the simulation parameters, we selected fine meshing which generated the design with mesh density of 900,000 elements and solved it multiple times (by changing boundary conditions to avoid changes

in thresholds). Final output was generated. The methodology was modified from Bourguignon et al. (Bourguignon et al. 2018).

In vitro biofilm formation and susceptibility assay

Pseudomonas aeruginosa PA01-EGFP was used to form the biofilms in 96-well microplates. The 96-well plate was inoculated with 100 µL of a 1/100 dilution of an exponential phase culture (0.01 optical density) for 48 h at 37 °C. After 48 h incubation, the plate was washed with PBS, and different concentrations (1.25, 2.50, and 5 µg/mL) of SNP, CNP, and CSNP were added to the wells (4×) and incubated for different time points (e.g., for 3, 6, and 24 h) at 37 °C. Lastly, the luminescence was measured using Synergy H1Hybrid Multi-Mode Reader (BioTek Instruments, USA). This experiment was performed in triplicate.

In vitro microfluidic assay for studying the efficacy of antibacterial nanoparticles under dynamic condition

The empty microchannels were exposed to oxygen plasma for 3 min to make PDMS more hydrophilic. The oxygen plasma was produced by BD-10A High-frequency generator (Electro-Technic Products, USA), the point electrode tip was placed in the inlet of the microchannel, and a needle was positioned in the outlet to ensure the treatment with high voltage (45,000 V) and frequency (500 kHz) of the entire length of the microchannel. Then, the microchannels were filled with 70% ethanol to remove any bubble in the microchannel. After that, 0.5 M NaOH for 30 min was used to disinfect and 4 mL of sterile water to rinse. Biofilms were cultured under hydrodynamic (laminar) conditions using a microfluidic device schematized in Fig. 1.

P. aeruginosa PA01-EGFP was inoculated into LB medium as pre-inoculum and incubated overnight at 37 °C at 200 rpm. The culture was then diluted in fresh LB (OD 0.05) and was flowed from the inlet well through the channel at the flow rates of 50, 75, 100, and 150 µl/min at 37 °C for 48 h.

After the biofilm was obtained in the microchips, it was treated with SNP, CNP, and CSNP at 1.25 µg/mL for 6 h phosphate buffer (pH 7) was used to flow in the microchips with biofilm as a control condition.

Assessing biofilm susceptibility using fluorescence microscopy

After biofilm growth and treatment, the biofilms were stained using a mixture of 10 µL each of the SYTO9 (Thermo Fisher), a green fluorescent nucleic acid stain for live cells and propidium iodide (red dead cells) stains introduced at a flow rate of 20 µL/h per channel. The biofilms were then imaged using an FSX100 inverted fluorescence microscope (Olympus, USA); images were captured at three different spots per channel with 100× and 42× magnification. The images were analyzed using the Fiji platform (Rueden et al. 2017). Using ImageJ, the intensity of the green and red fluorescence was measured at 6 different locations in the captured image keeping a constant area, and an average value was calculated. The graphs are plotted using the calculated intensity to give a semiquantitative analysis of the effect of the NPs.

Statistical analysis

ANOVA and Tukey's tests were used to perform statistical analysis with the significance level set at $p < 0.05$.

Results

Fabrication of the chip and flow simulations

The fabricated microchip was connected to a syringe pump, and a test run was conducted with 1×PBS (phosphate buffer saline) solution to check for probable leaks and formation of air bubbles. It was found that the design of the chip does not allow for the formation of air bubbles and obstruction of fluid flow and, therefore, most suitable for long study (in our case, seven days). The flow velocity pattern shows a gradient of increasing flow rates from 50 to 150 µL/min (Fig. 2). The flow rate increases the velocity at the periphery and the junction of two chambers compared to other locations, which suggests a higher shear rate at these locations. High flow velocities have been reported (Park et al. 2011) to be advantageous to the establishment of bacterial biofilm and also induces anchorage-dependent proteins. The higher shear has also been reported to aid in bacterial growth and establishing new colonies (Rizk et al. 2019). We conclude that a flow rate of 150 µL/min was optimal to obtain and study the bacterial biofilm from these studies.

Characterization of the nanoparticles

The synthesized nanoparticles (SNP, CNP, and CSNP) were characterized for size, shape, and charge (Fig. 3a). Absorbance spectra of SNP show a redshift as size increases (Fig. 3a). Visually, the CSNP particles are darker yellow in color. All the nanoparticles are within the nano range in size (Fig. 3b). The SNPs showed the smallest size (23 nm), whereas the CNPs were the largest size (152 nm). The latter could be due to agglomeration formation, while when complexing with silver. The size of the CSNP is smaller (48 nm), which would increase their antibiofilm activity by (a) increasing the surface of

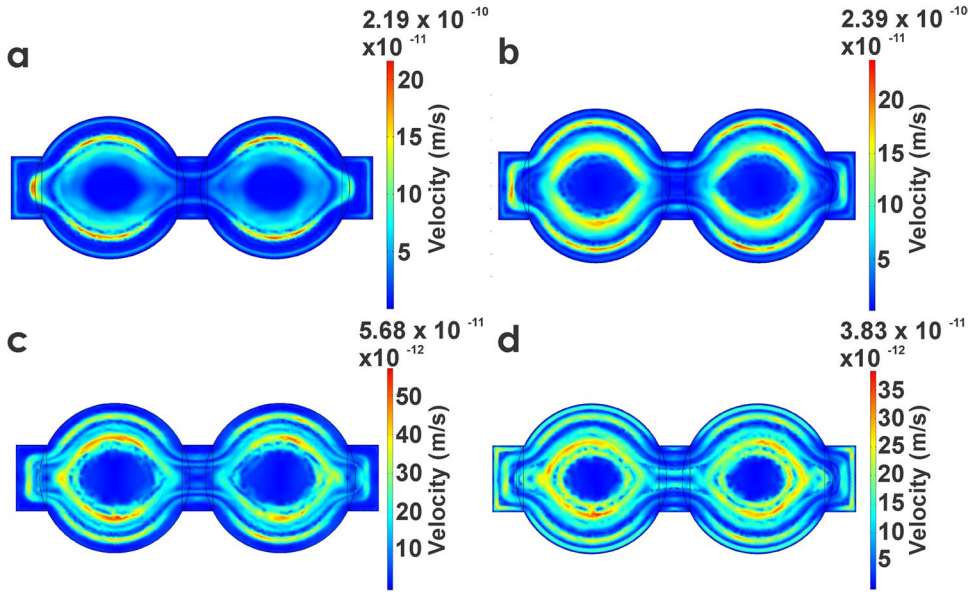

Fig. 2 Computational flow simulation. Simulation output from COMSOL showing a graphical representation of flow velocity at different flow rates: **a** 50 µL/min, **b** 75 µL/min, **c** 100 µL/min, and **d** 150 µL/min

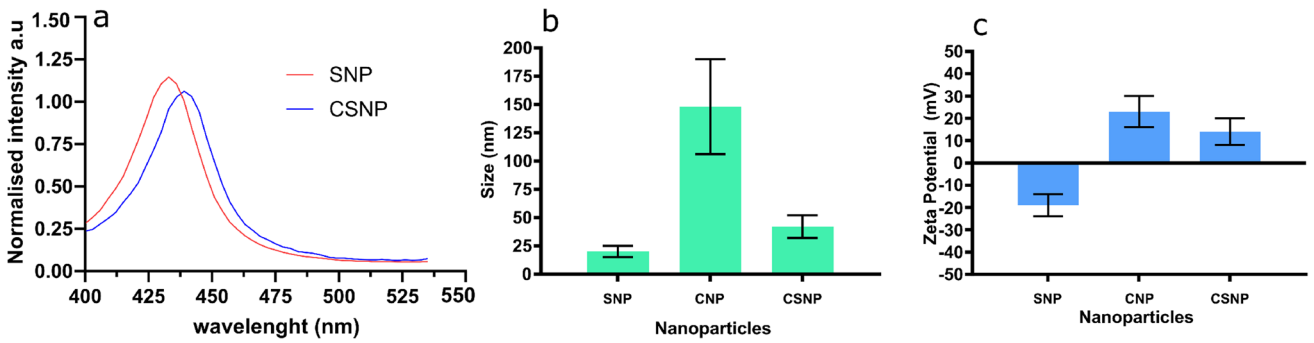

Fig. 3 Characterization of nanoparticles. **a** Absorbance spectra, **b** Size, and **c** Zeta potential determined using Malvern size analyzer. SNP silver nanoparticles, CNP chitosan nanoparticles, and CSNP chitosan-coated silver nanoparticles

contact with the biofilm as smaller size of nanoparticles is associated with offering large surface to volume ratio, and (b) smaller size of nanoparticles shows more adherence and uptake by cells. The zeta potentials for SNP and CNP and CSNP are − 18 mV ± 5, CNP + 22 mV ± 7, and CSNP + 12 mV ± 6, respectively (Fig. 3c). The binding of silver nanoparticles with free amino group in chitosan is further confirmed by the lower zeta potential value of the silver-loaded chitosan nanoparticles. The negative zeta potential is due to the nature of the reduction reaction process, which involves sodium borohydride and trisodium citrate, which act as capping agent imparting net negative charge. In all the following 3 cases SNP, CNP and CSNP have shown antibacterial activity in non-dynamic environment, but activity in dynamic continuous flow has not been explored fully in terms of particle flow, adherence, and uptake in living systems.

Assessing biofilm formation and flow rate optimization

This microfluidic chip is designed to reduce the variance of in vitro biofilms' growth while providing integrated high control; consequently, it enables more reliable assessments of new treatments for biofilm on a single device (Subramanian et al. 2016). The microfluidic device allows the ability to get a high spatiotemporal resolution and live-cell imaging. PDMS was selected as a manufacturing microchip material, and it brings many advantages as easy to use, transparency, biocompatibility, and gas permeability (Burmeister et al. 2019). To form a mature biofilm in the microchannels to be exposed at the different treatments, four flow rates were evaluated: 50, 75, 100, and 150 µL/min (Fig. 4). The difference in the architecture biofilms grown under the different flow rates after two days was evaluated (Fig. 4a). Biofilm

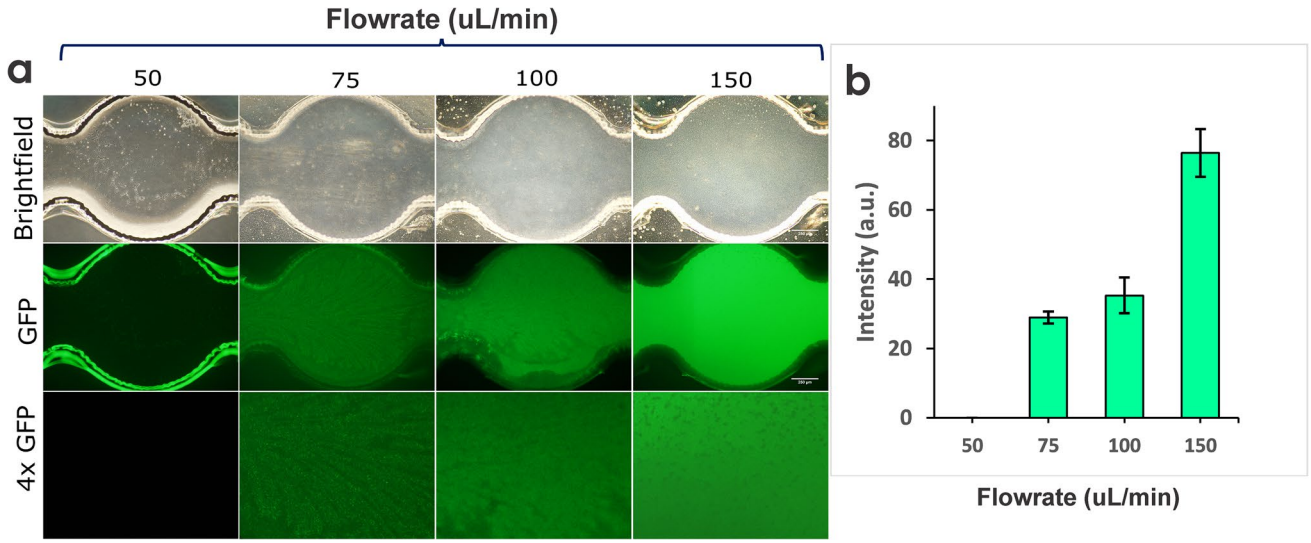

Fig. 4 Formation of *P. aeruginosa* PA01-EGFP biofilm at different flow rates in the microfluidic device. **a** Representative fluorescence microscopic images of the biofilm and **b** fluorescence intensity of biofilm growth at different flow rates

data reveals the development of different morphologies involving cover and shape depending on flow velocities in the microchannels. Reduced biofilm growth at the lowest flow rate (50 µL/min) was observed. The biofilm showed a fluid streamline pattern in the microchannel in the flow direction at intermediate flow rates (75 and 100 µL/min). Furthermore, a more robust biofilm, denser, thicker, and more homogeneous architecture, was observed at the highest flow tested that was 150 µL/min (Fig. 4). Figure 5 shows SEM images of the biofilm grown in the microchannels.

Biofilm inhibition properties of the nanoparticles

The NPs are reactive entities that can easily penetrate into a biofilm matrix that often behaves as a barrier for many antibiotics (Qayyum and Khan 2016). This study shows a concentration-dependent reduction in biofilm formation (i.e., antibiofilm activity) of all the tested nanoparticles (e.g., SNP, CNP, and CSNP) indicated by the loss of fluorescence (Fig. 6). The fluorescence at time 0 for all the treatments was 100%. SNP and CSNP resulted > 50% biofilm reduction after 3 h at all concentrations, and CNP showed > 40% biofilm reduction at 6 h for 2.5 µg/mL and 5 µg/mL. As the duration of CSN treatment time increased, there was a decrease in the fluorescence signal, indicating inhibition. According to these results, the 6-h treatment time, because at this time the highest attenuation of GFP (green) intensity, and the concentrations (1.25 µg/mL) of NPs were selected to evaluate the antibiofilm effect under continuous flow in microfluidic devices.

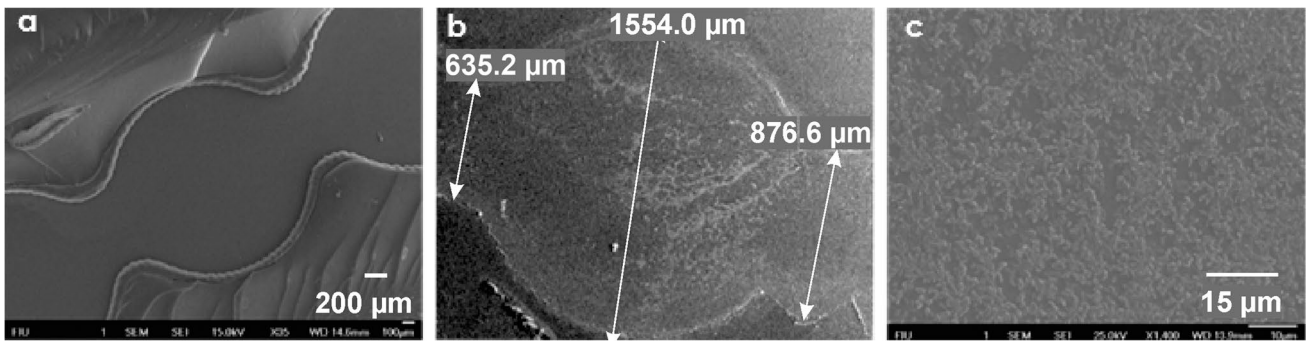

Fig. 5 SEM images. **a** Microchamber in the chip, **b** 2-day-old bacterial biofilm, and **c** magnified image of bacterial biofilm in the microchannels growing in continuous flow

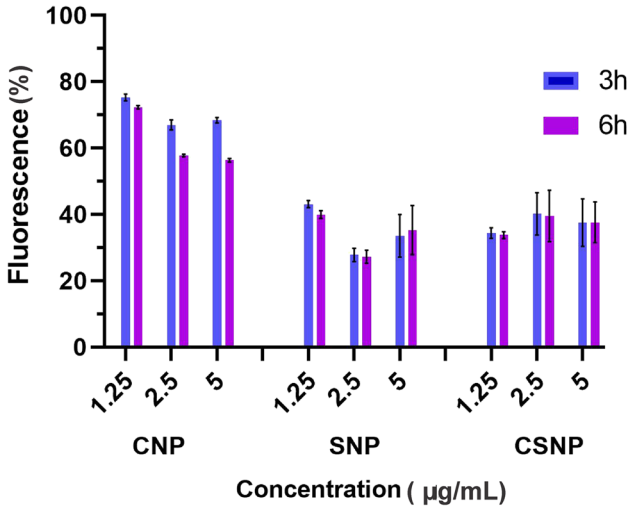

Fig. 6 Inhibition effects of nanoparticles on matured biofilm growth on 96-well microplate

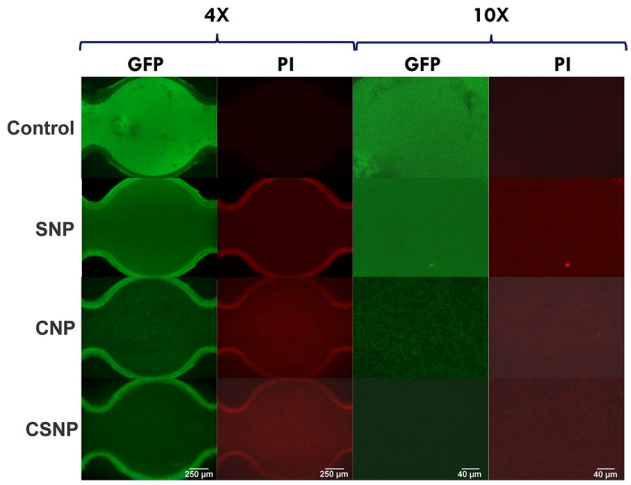

Fig. 7 Screening of antibiofilm activity of nanoparticles in the microfluidic device. Representative fluorescence microscopic images of *P. aeruginosa* PA01-EGFP biofilm exposed with SNP, CNP and CSNP. Microphotographs with 4×and 10×magnification. Live cells are shown in green fluorescence, and dead cells are marked with propidium iodide with red fluorescence

Antibiofilm effect of SNP, CNP, and CSNP in a continuous flow

The microfluidic flow chamber biofilms closely mimic in vivo conditions during infections (Lebeaux et al. 2013; Brackman and Coenye 2015). The impacts of SN, CNP, and CSNP on the biofilm architecture and cell morphology were determined using fluorescence microscopy (Fig. 7). A 2-day-old formed *P. aeruginosa* biofilm was treated with the NPs (at 1.25 µg/mL) and with saline solution as a control for 6 h. The formed biofilm decreased simultaneously in biomass and live/dead cell relationship (Fig. 7; Table 1). The live/dead relationship was established according to the signals' intensity in the microchannels' cisterns. Control biofilm without NPs treatment (buffer) exhibited the highest live/death ratio value of 6.15 (live cells/green intensity: 51.87 ± 1.16 and dead cells/red intensity: 8.42 ± 0.02). A significant reduction in the biomass live/dead cells ratio ($p < 0.05$) was detected after the addition of SNP, CNP, and CSNP (Table 1). The highest (%) reduction was observed with CSNP compared to the control.

Semiquantitative analysis of the images by live/dead cells intensity measurement estimates bacterial detachment of 65.5% from the biofilm after CSNP treatment. In comparison, it was 59% and 51% for CNP and SNP, respectively. Slight differences were observed between SNPs and the control group. However, treatment with CSNP enlisted the inhibition with only 0.45 live/dead cells. While chitosan alone (CNP) showed a reasonable extent of biofilm eradication, its antibacterial activity was significantly improved in the presence of SNP. This could be due to the release of silver ion from silver-loaded chitosan nanoparticles and or the combined activity of chitosan and silver nanoparticles (Ali et al. 2011).

Discussion

Bacteria quickly develop different mechanisms that allow adapting to the environment in which they live. The ability of bacterial pathogens to establish biofilm structures is considered an important virulence factor associated with the disease's persistence, allowing bacteria to avoid host immune response and antibiotic treatment (Soledad et al. 2019). On the other hand, it has been proposed that robust biofilm was formed as an adaptive response to increase bacteria survival under stress conditions like high shear stress, so biofilm tends to develop in presence of the most increased shear stress value (Rizk et al. 2019). Multilayer structure morphology of the biofilms grown in a nutrient broth (LB in this work) under flow conditions has been previously observed (Kanthawong et al. 2018; Yang et al. 2019).

In this context, microfluidics have involved a rapidly growing attention in the imitation of biological phenomena by providing identical and reproducible natural conditions, addressing unprecedented control over the flow conditions, as well as real-time observation (Liu et al. 2019b). A high-throughput microfluidic platform was developed for screening drugs under continuous-flow conditions that closely mimic the in vivo conditions. Previous reports have explored the use of microfluidics for examining biofilm formation at pore scale under various hydrodynamic conditions (Liu et al. 2019a). The developed LOC technology offers advantages as a closed system where bacterial

Table 1 Image analysis of the biofilm treated with different nanoparticles. Values of fluorescent green intensity (live cells), red intensity (dead cells) and their relationship (live/dead cells)

	Live cells (a.u.)	Dead cells (a.u)	Live/dead cells
Control	51.87 ± 1.16	8.42 ± 0.02	6.15
Silver NP (SNP)	25.62 ± 0.60*	16.36 ± 0.37*	1.57
Chitosan NP (CNP)	21.25 ± 0.35*	24.87 ± 0.18*	0.85
Chitosan-silver NP (CSNP)	17.86 ± 0.34*	39.84 ± 0.85*	0.45

Two-day biofilms were treated with 1.25 µg/mL nanoparticles. Values indicate the amount of live and dead cells (green and red fluorescence, respectively, in the assay) inside the biofilm. Values represent the mean ± SD from six random areas

*Significant differences compared to control (non-treated) biofilm ($p < 0.05$, Student's t test)

NP nanoparticle

biofilms can interact with hydrodynamic environments (for example, shear stress) (Kim et al. 2012).

We observed that the best properties and highest efficiency in biofilm formation were obtained at the highest flow rate (150 µL/min). Our results agree with those of Liu et al. (Liu et al. 2019b), who reported that biofilm accumulation in microchannels increased with flow rate and shear stress. The higher shear appears optimal for biofilm growth, possibly because the media is provided with more nutrients so that the biofilm can propagate more rapidly (Sutlief et al. 2019) and increase its metabolic rate (Jones and Buie 2019).

Here, we proposed the first comparative report on the usage of SNP, CNP, and CSNP for eradicating pre-formed matured biofilm of *P. aeruginosa* evaluated in a continuous flow using a microfluidics system. The results showed high inhibitory activity of SNP, which is also evident in the traditional assay as silver nanoparticles are more toxic and act via releasing silver ions which damage oxidative mitochondrial pathway and in turn cell machinery. In the case of chitosan nanoparticles in continuous flow allows better interaction with bacterial cells. There are two possible mechanisms for chitosan toxicity: (a) the interaction of positive charged chitosan nanoparticles with negative charged cell membranes causes a leakage of cellular plasma and proteins and its internalization causes damage to the microbial DNA and (2) chitosan nanoparticles interfere with protein synthesis (Khan et al. 2019; Baelo et al. 2015).

In the case of CSNP, which showed a greater inhibitory effect of biofilm of 65.5%, chitosan helps in adherence to bacterial cells, and silver nanoparticles promote ion leaching, and this dual effect causes maximum killing activity. Also, the dual nature of chitosan and silver nanoparticles is advantageous in dislodging the biofilm via adhering in the biofilm matrix in continuous flow, and silver ion leaching acts by killing localized cells. The modification can work in synergy for an array of nanoparticle combinations which can have dual activity in inhibiting a wide range of bacterial biofilm. Further studies have to be conducted to clarify the mechanism of biofilm inhibition and reduction of virulence factors by CSNP in *P. aeruginosa* at the molecular level.

In conclusion, this study shows that the LOC proposed as a dynamic culture system allows a good biofilm formation and is a valuable fast and low-cost tool for quickly screening the antimicrobial activity of nano-drugs in biofilms. This microchip can be used in drug testing for clinical applications. In addition, it may be useful for studying cell–cell interaction and biofilm-drug/nanoparticle response. The small volume applied compared to other systems makes it suitable for screening of biofilm inhibitors in continuous flow. It was also observed that in such a dynamic environment, the biofilm is much more sensitive to treatment groups as compared to traditional plate assay and is closer to the natural environment. With this setup, a lower dose is required to achieve the same effect as traditional static cultures.

The high efficacy in the biofilm inhibition using a microfluidic device would be explained due to the continuous replenishment of the NPs in the miniaturized microenvironment. The use of this innovative tool is highly promising for screening the treatment and prevention against the formation of antibiotic-resistant biofilm infection, in clinical and environmental situations.

In conclusion, this work provides a detailed description of a microfluidic platform to improve the study of *P. aeruginosa* biofilms. The technology could easily be extended to biofilms of other strains of bacteria, fungi, or algae. The platform can be used as an excellent system to study drug susceptibility and screenings assays using low doses. The results are encouraging and pave the way for the screening of more types of carriers and combinations of antimicrobial compounds to treat resistant bacterial infections. In addition, among the possible applications of the system would be to study the treatment of biofilm infections in wounds, medical implants such as urinary catheters and artificial joints, and in environmental biofilms such as those found in water pipes and biofouling.

Author contribution NB and VK studied the conception and design, performed the experiments, analysis, and interpretation of data, and writing — original draft preparation. MP designed the microdevice, performed investigation, and critical revision. KM and BL contributed to the conceptualization, research, critical revision, and writing — review and editing. SB provided the visualization, supervision, and writing — review and editing. All the authors offered intellectual inputs, read, and approved the manuscript.

Funding This study was funded by CONICET (grant number PICT 2018–01421) and National Institute on Minority Health and Health Disparities of the National Institutes of Health (Pilot Award Number 800013656).

Data availability The datasets generated during and/or analyzed during the current study are available from the corresponding author on reasonable request.

Declarations

Ethics approval This article does not contain any studies with human participants or animals performed by any of the authors.

Conflict of interest The authors declare no competing interests.

Disclaimer The content is solely the authors' responsibility and does not necessarily represent the official views of the National Institutes of Health.

References

Affes S, Maalej H, Aranaz I, Kchaou H, Acosta N, Heras Á, Nasri M (2020) Controlled size green synthesis of bioactive silver nanoparticles assisted by chitosan and its derivatives and their application in biofilm preparation. Carbohydr Polym 236:116063. https://doi.org/10.1016/j.carbpol.2020.116063

Ali SW, Rajendran S, Joshi M (2011) Synthesis and characterization of chitosan and silver loaded chitosan nanoparticles for bioactive polyester. Carbohydr Polym 83:438–446. https://doi.org/10.1016/j.carbpol.2010.08.004

Andersson DI (2003) Persistence of antibiotic resistant bacteria. Curr Opin Microbiol 6:452–456. https://doi.org/10.1016/j.mib.2003.09.001

Baelo A, Levato R, Julián E, Crespo A, Astola J, Gavaldà J, Engel E, Mateos-timoneda MA, Torrents E (2015) Disassembling bacterial extracellular matrix with DNase-coated nanoparticles to enhance antibiotic delivery in bio fi lm infections. J Control Release 209:150–158. https://doi.org/10.1016/j.jconrel.2015.04.028

Benoit DSW, Sims KR, Fraser D (2019) Nanoparticles for oral biofilm treatments. ACS Nano 13:4869–4875. https://doi.org/10.1021/acsnano.9b02816

Bourguignon N, Attallah C, Karp P, Booth R, Peñaherrera A, Payés C, Oggero M, Pérez MS, Helguera G, Lerner B (2018) Production of monoclonal antibodies in microfluidic devices. Integr Biol (camb) 10(3):136–144. https://doi.org/10.1039/c7ib00200a

Bowler P, Murphy C, Wolcott R (2020) Biofilm exacerbates antibiotic resistance: is this a current oversight in antimicrobial stewardship? Antimicrob Resist Infect Control 9:1–5. https://doi.org/10.1186/s13756-020-00830-6

Brackman G, Coenye T (2015) In vitro and in vivo wound models. Advances in Microbiology, Infectious Diseases and Public Health. Advances in Experimental Medicine and Biology, vol 897. .https://doi.org/10.1007/5584_2015_5002

Brandenburg KS, Weaver AJ Jr, Qian L, You T, Chen P, Karna SLR, Fourcaudot AB, Sebastian EA, Abercrombie JJ, Pineda U et al (2018) Development of *Pseudomonas aeruginosa* biofilms in partial-thickness burn wounds using a sprague-dawley rat model. J Burn Care Res 40(1):44–57. https://doi.org/10.1093/jbcr/iry043

Burmeister A, Hilgers F, Langner A, Westerwalbesloh C, Kerkhoff Y, Tenhaef N, Drepper T, Kohlheyer D, Von Lieres E, Noack S, Grünberger A (2019) A microfluidic co-cultivation platform to investigate microbial interactions at defined microenvironments. Lab Chip 19:98–110. https://doi.org/10.1039/c8lc00977e

Choudhury H, Pandey M, Lim YQ, Low CY, Lee CT, Marilyn TCL, Loh HS, Lim YP, Lee CF, Bhattamishra SK, Kesharwani P, Gorain B (2020) Silver nanoparticles: advanced and promising technology in diabetic wound therapy. Mater Sci Eng C 112:110925. https://doi.org/10.1016/j.msec.2020.110925

Coenye T, Peeters E, Nelis HJ (2007) Biofilm formation by Propionibacterium acnes is associated with increased resistance to antimicrobial agents and increased production of putative virulence factors. Res Microbiol 158:386–392. https://doi.org/10.1016/j.resmic.2007.02.001

Drago F, Gariazzo L, Cioni M, Trave I, Parodi A (2019) The microbiome and its relevance in complex wounds. Eur J Dermatology 29(1):6–13. https://doi.org/10.1684/ejd.2018.3486

Ganem-Rondero A, Sanchez-Sanchez R, Alvarado-Gomez E, Martínez-Castañon G, Martinez-Gutierrez F, Yacaman MJ (2018) Evaluation of anti-biofilm and cytotoxic effect of a gel formulation with Pluronic F-127 and silver nanoparticles as a potential treatment for skin wounds. Mater Sci Eng C 92:621–630. https://doi.org/10.1016/j.msec.2018.07.023

Illath K, Kar S, Gupta P, Shinde A, Wankhar S, Tseng FG, Lim KT, Nagai M, Santra TS (2021) Microfluidic nanomaterials: from synthesis to biomedical applications. Biomaterials 280:121247. https://doi.org/10.1016/j.biomaterials.2021.121247

Jones AD, Buie CR (2019) Continuous shear stress alters metabolism , mass-transport , and growth in electroactive biofilms independent of surface substrate transport. Sci Rep 1–8. https://doi.org/10.1038/s41598-019-39267-2

Kamat V, Bodas D, Paknikar K (2016) Chitosan nanoparticles synthesis caught in action using microdroplet reactions. Sci Rep 6:1–4. https://doi.org/10.1038/srep22260

Kanthawong S, Chareonsudjai S, Taweechaisupapong S (2018) Impact of nutritional stress on drug susceptibility and biofilm structures of *Burkholderia pseudomallei* and *Burkholderia thailandensis* grown in static and microfluidic systems. PLoS One 1–18. https://doi.org/10.1371/journal.pone.0194946

Khan F, Manivasagan P, Thuy D, Pham N, Oh J, Kim S, Kim Y (2019) Microbial pathogenesis antibiofilm and antivirulence properties of chitosan-polypyrrole nanocomposites to *Pseudomonas aeruginosa*. Microb Pthogenes 128:363–373. https://doi.org/10.1016/j.micpath.2019.01.033

Kim J, Park HD, Chung S (2012) Microfluidic approaches to bacterial biofilm formation. olecules 17: (8) 9818–9834. https://doi.org/10.3390/molecules17089818

KLayout (2018) High performance layout viewer and editor. 2018. Available Online Http//www.klayout.de/index.php

Kyzioł K, Kaczmarek L, Kyzioł A (2017) Surface functionalization of biomaterials. Handbook of Composites from Renewable Materials 4:457–490

Lebeaux D, Chauhan A, Rendueles O, Beloin C (2013) From in vitro to in vivo models of bacterial biofilm-related infections. Pathogens 2:288–356. https://doi.org/10.3390/pathogens2020288

Liu N, Skauge T, Landa-Marbán D, Hovland B, Thorbjørnsen B, Radu FA, Vik BF, Baumann T, Bødtker G (2019a) Microfluidic study of effects of flow velocity and nutrient concentration on biofilm

accumulation and adhesive strength in the flowing and no-flowing microchannels. J Ind Microbiol Biotechnol 46:855–868. https://doi.org/10.1007/s10295-019-02161-x

Liu N, Skauge T, Landa D, Beate M, Bente H, Florin T, Radu A (2019b) Microfluidic study of effects of flow velocity and nutrient concentration on biofilm accumulation and adhesive strength in the flowing and no - flowing microchannels. J Ind Microbiol Biotechnol 46(6):855–868. https://doi.org/10.1007/s10295-019-02161-x

Maurice NM, Bedi B, Sadikot RT (2018) *Pseudomonas aeruginosa* biofilms: host response and clinical implications in lung infections. Am J Respir Cell Mol Biol 58:428–439. https://doi.org/10.1165/rcmb.2017-0321TR

Mulcahy LR, Isabella VM, Lewis K (2014) *Pseudomonas aeruginosa* Biofilms in Disease. Microb Ecol 68:1–12. https://doi.org/10.1007/s00248-013-0297-x

Negut I, Grumezescu V, Grumezescu AM (2018) Treatment strategies for infected wounds. Molecules 23:1–23. https://doi.org/10.3390/molecules23092392

Park A, Jeong H, Lee J, Kim KP, Lee C (2011) Effect of Shear Stress on the Formation of Bacterial Biofilm in a Microfluidic Channel 5:236–241. https://doi.org/10.1007/s13206-011-5307-9

Peñaherrera A, Payés C, Sierra-Rodero M, Vega M, Rosero G, Lerner B, Helguera G, Pérez MSS (2016) Evaluation of cell culture in microfluidic chips for application in monoclonal antibody production. Microelectron Eng 158:126–129. https://doi.org/10.1016/j.mee.2016.03.059

Qayyum S, Khan AU (2016) Nanoparticles: vs. biofilms: a battle against another paradigm of antibiotic resistance. Medchemcomm 7:1479–1498. https://doi.org/10.1039/c6md00124f

Rizk N, Ait-Mouheb N, Molle B, Roche N (2019) Treated wastewater reuse in micro-irrigation: effect of shear stress on biofilm development kinetics and chemical precipitation. Environ Technol (United Kingdom) 0:1–11. https://doi.org/10.1080/09593330.2019.1625956

Rueden CT, Schindelin J, Hiner MC, DeZonia BE, Walter AE, Arena ET, Eliceiri KW (2017) Image J2: ImageJ for the next generation of scientific image data. BMC Bioinformatics 18:1–26. https://doi.org/10.1186/s12859-017-1934-z

Singh N, Rajwade J, Paknikar KM (2019) Transcriptome analysis of silver nanoparticles treated *Staphylococcus aureus* reveals potential targets for biofilm inhibition. Colloids Surfaces B Biointerfaces 175:487–497. https://doi.org/10.1016/j.colsurfb.2018.12.032

Soledad M, Isaac P, Laura M, Paola L (2019) Chitosan nanoparticles enhance the antibacterial activity of the native polymer against bovine mastitis pathogens. Carbohydr Polym 213:1–9. https://doi.org/10.1016/j.carbpol.2019.02.016

Souza JGS, Bertolini MM, Costa RC, Nagay BE, Dongari-Bagtzoglou A, Barão VAR (2021) Targeting implant-associated infections: titanium surface loaded with antimicrobial. iScience 24: (1) 102008. https://doi.org/10.1016/j.isci.2020.102008

Spittaels KJ, Coenye T (2018) Developing an in vitro artificial sebum model to study *Propionibacterium acnes* biofilms. Anaerobe 49:21–29. https://doi.org/10.1016/j.anaerobe.2017.11.002

Stanley CE, Grossmann G, Casadevall i Solvas X, de Mello AJ, (2016) Soil-on-a-chip: microfluidic platforms for environmental organismal studies. Lab Chip 16(2):228–241. https://doi.org/10.1039/C5LC01285F

Stücker M, Baier V, Reuther T, Hoffmann K, Kellam K, Altmeyer P (1996) Capillary blood cell velocity in human skin capillaries located perpendicularly to the skin surface: measured by a new laser Doppler anemometer. Microvasc Res 52:188–192. https://doi.org/10.1006/mvre.1996.0054

Subhadra B, Kim DH, Woo K, Surendran S, Choi CH (2018) Control of biofilm formation in healthcare: recent advances exploiting quorum-sensing interference strategies and multidrug efflux pump inhibitors. Materials (basel) 11(9):1676. https://doi.org/10.3390/ma11091676

Subramanian S, Gerasopoulos K, Guo M (2016) Autoinducer-2 analogs and electric fields - an antibiotic-free bacterial biofilm combination treatment. Biomed Microdevices 1–12. https://doi.org/10.1007/s10544-016-0120-9

Sutlief AL, Valquier-Flynn H, Wilson C, Perez M, Kleinschmidt H, Schofield BJ, Delmain E, Holmes AE, Wentworth CD (2019) Live cell analysis of shear stress on *Pseudomonas aeruginosa* using an automated higher-throughput microfluidic system. JoVE (Journal Vis Exp) 143:e58926. https://doi.org/10.3791/58926

Thi MTT, Wibowo D, Rehm BHA (2020) *Pseudomonas aeruginosa* biofilms. Int J Mol Sci 21:1–25. https://doi.org/10.3390/ijms21228671

Vu XH, Duong TTT, Pham TTH, Trinh DK, Nguyen XH, Dang VS (2018) Synthesis and study of silver nanoparticles for antibacterial activity against *Escherichia coli* and *Staphylococcus aureus*. Adv Nat Sci Nanosci Nanotechnol 9(2):025019. https://doi.org/10.1088/2043-6254/aac58f

Whitesides GM (2006) The origins and the future of microfluidics. Nature 442(7101):368–373. https://doi.org/10.1038/nature05058

Wu H, Song Z, Hentzer M, Andersen JB, Heydorn A, Mathee K, Moser C, Eberl L, Molin S, Hoiby N, Givskov M (2000) Detection of N-acylhomoserine lactones in lung tissues of mice infected with *Pseudomonas aeruginosa*. Microbiology 146:2481–2493. https://doi.org/10.1099/00221287-146-10-2481

Yang J, Cheng S, Li C, Sun Y, Huang H (2019) Shear stress affects biofilm structure and consequently current generation of bioanode in microbial electrochemical systems (MESS). Front Microbiol 10:1–8. https://doi.org/10.3389/fmicb.2019.00398